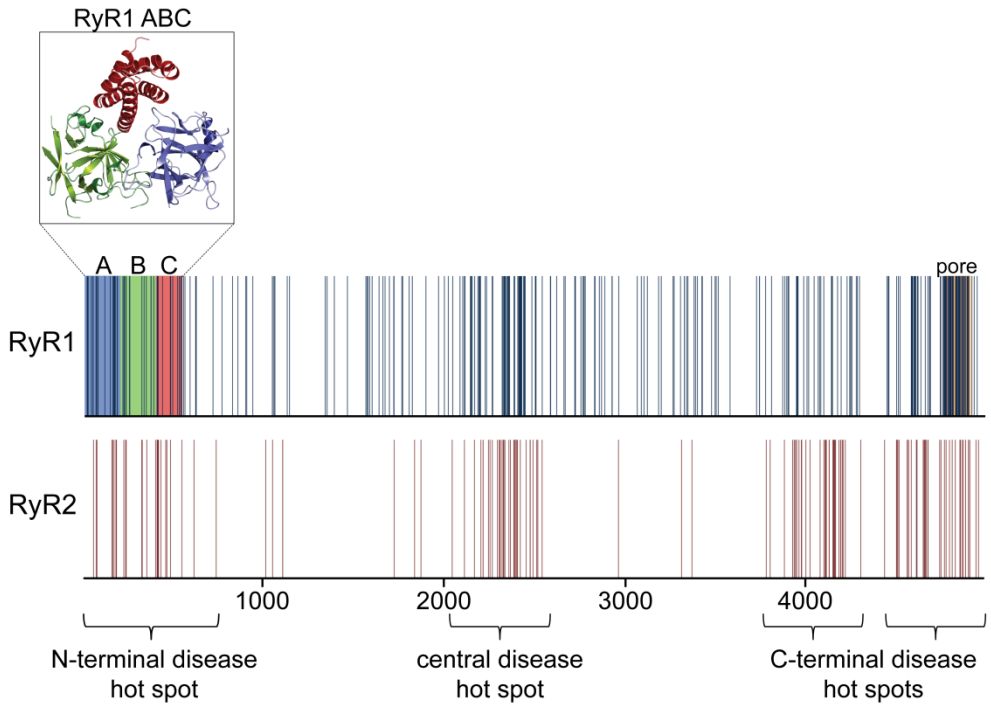

Supplementary Figure S1: Linear view of RyR1 and RyR2 disease mutations.

Amino acid numbers are shown below. Vertical lines indicate disease mutations. There is still a clear clustering of mutations in RyR2, but several mutations are increasingly found outside of the initially proposed hot spots for RyR1. The RyR1 N-terminal ABC domains and the pore-forming region are highlighted. The crystal structure of wild type RyR1ABC (PDB accession code 2XOA) is shown above.

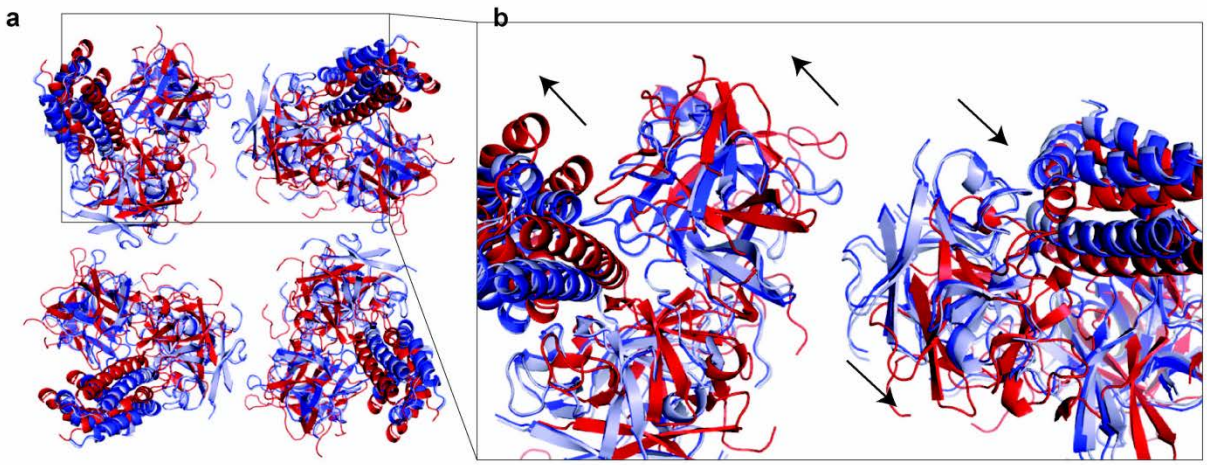

Supplementary Figure S2: RyR1ABC docking results for different cryo-EM maps

a) Comparison of docking results for RyR1ABC into two different closed RyR1 maps[14,30](EMD1606 - dark blue, EMD5014 - light blue) shows a near perfect superposition, indicating that the results for closed maps are consistent, with near identical intersubunit arrangements. The result for docking into the 9.6Å map EMD1275[15] (red) shows increased intersubunit distances like in the open RyR1 map EMD1607 (Figure 1). Initially presumed to represent a closed state, it was later suggested that EMD1275 may rather represent and open RyR1, or a mixture of different states[14]. The increased intersubunit distances for docking in EMD1275 would support this assumption. **b)** Close-up view with arrows indicating the shifts the models undergo from EMD1606 to EMD1275.

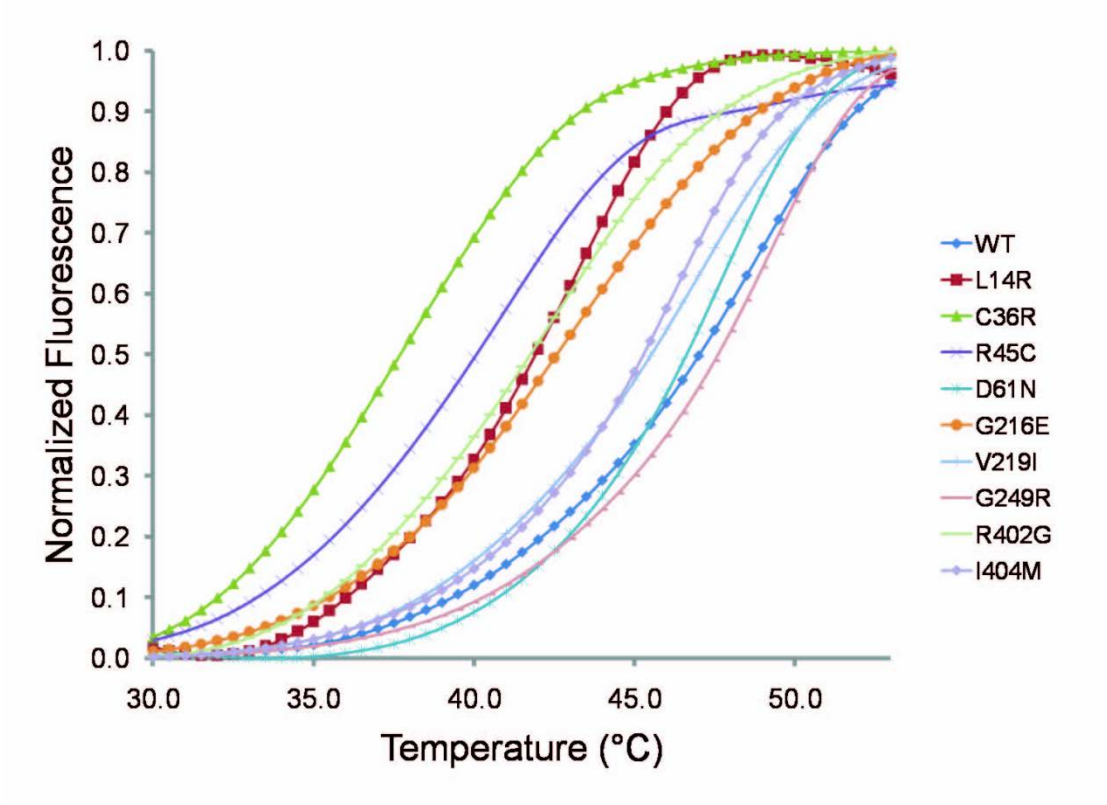

Supplementary Figure S3: Thermal melt analysis

Melting curves for wild-type RyR1ABC and nine different disease mutants using thermofluor experiments. The curves are the average of four measurements. The melting temperatures are defined as the midpoints of each transition. The average melting temperatures and corresponding errors are shown in Figure 3.

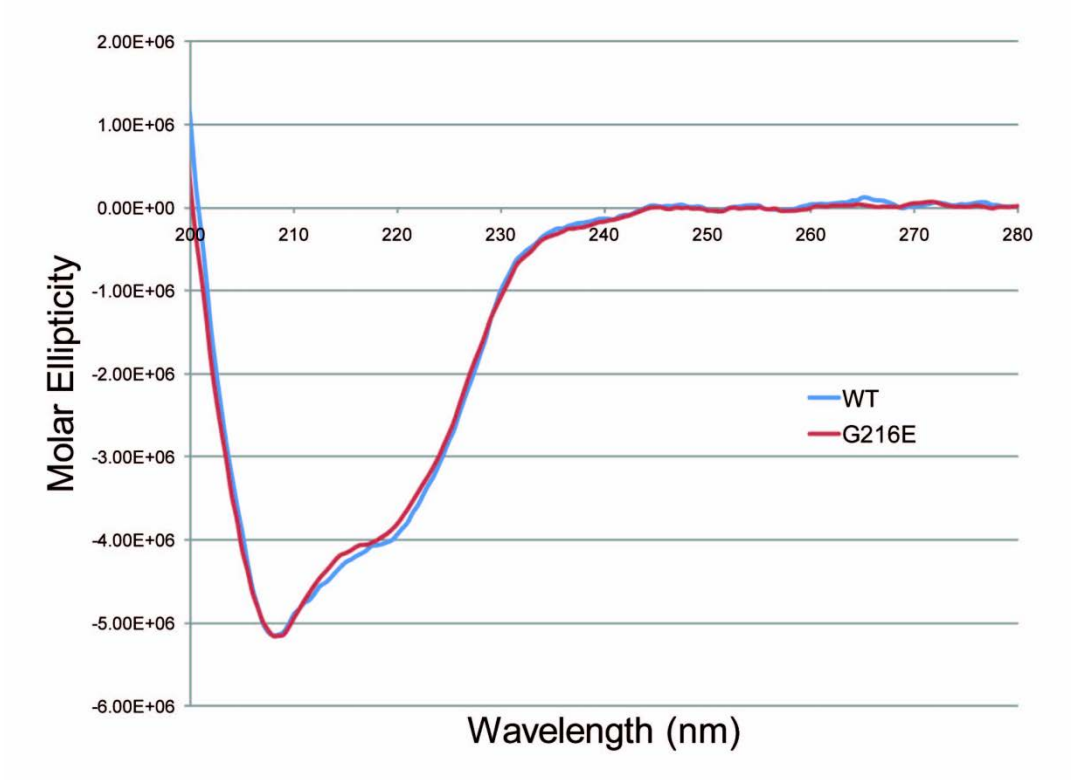

Supplementary Figure S4: Circular dichroism

The CD spectra for wild type and G216E RyR1ABC are very similar, suggesting that the disease mutation does not lead to changes in overall secondary structure content. This suggests that the inability of G216E to crystallize is likely due to relative domain movements or a generally increased flexibility of the domains relative to one another.

a

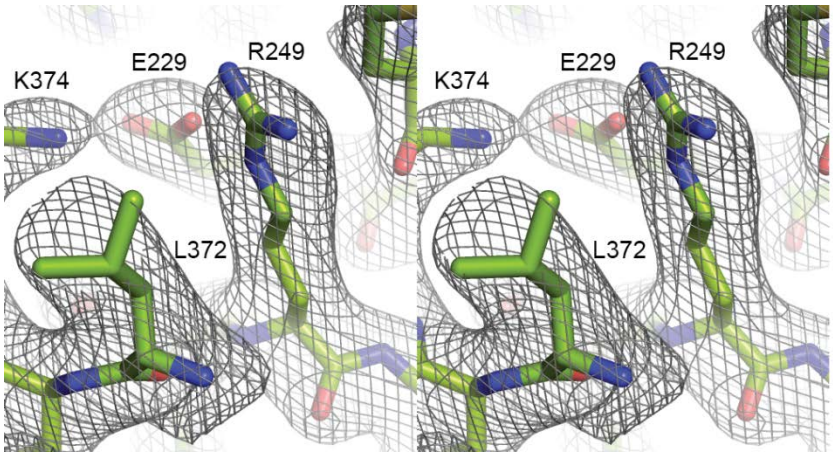
K374
E229
R249
L372
K374
E229
R249
L372

b

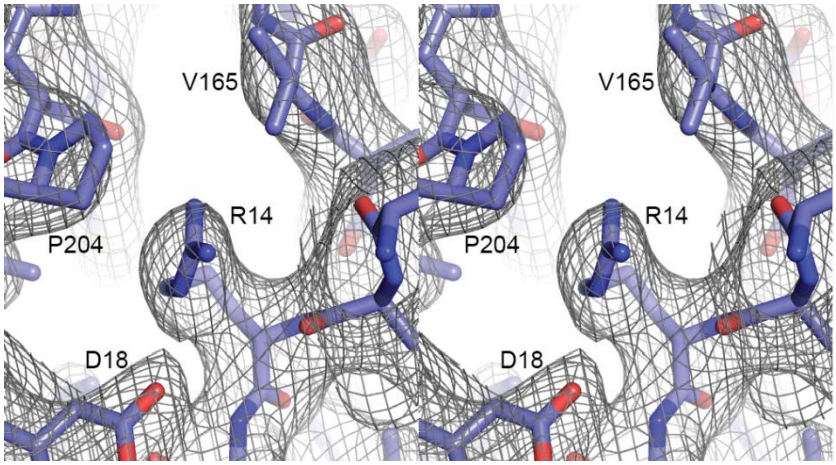
V165
R14
P204
D18
V165
R14
P204
D18

c

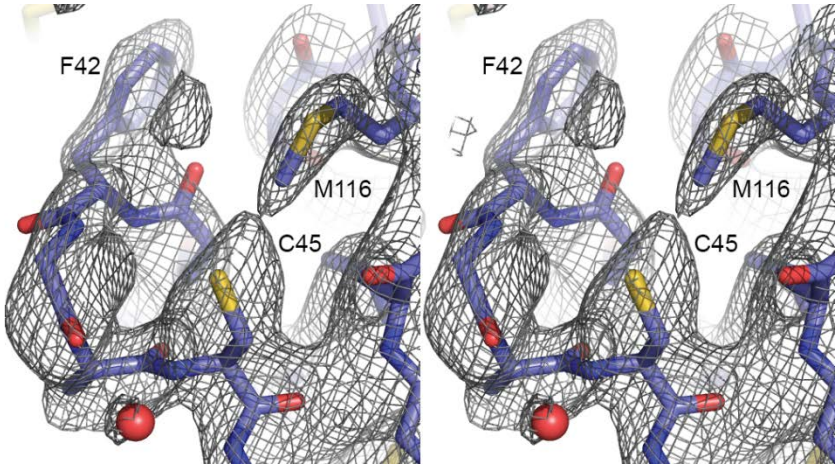
F42
M116
C45
F42
M116
C45

d

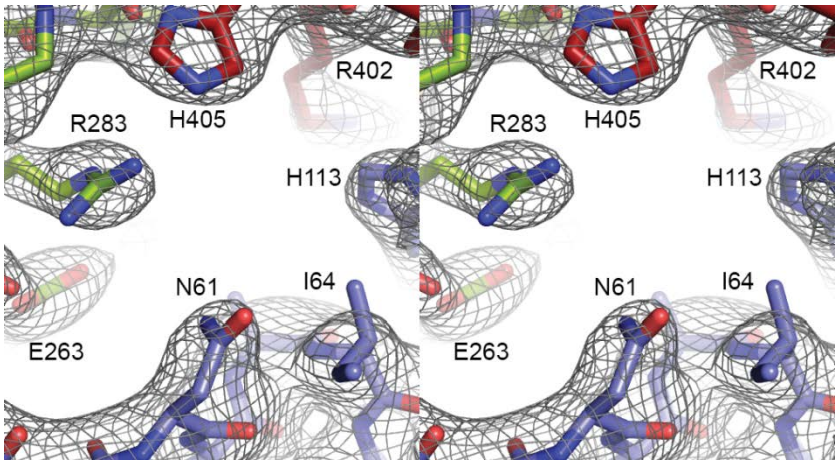
R402
R283
H405
H113
N61
I64
E263
R402
R283
H405
H113
N61
I64
E263

e

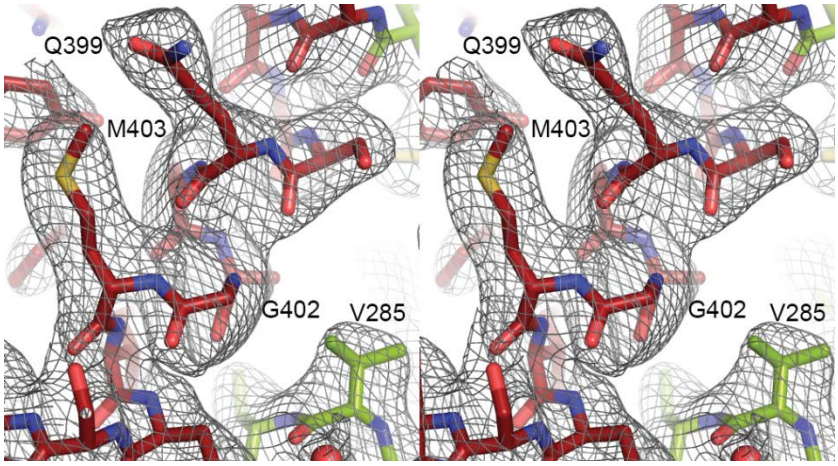
Q399
M403
G402
V285
Q399
M403
G402
V285

f

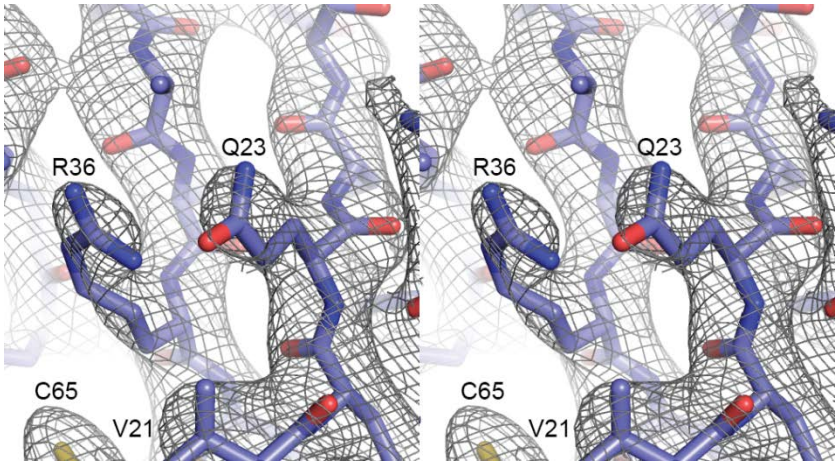
R36
Q23
C65
V21
R36
Q23
C65
V21

g

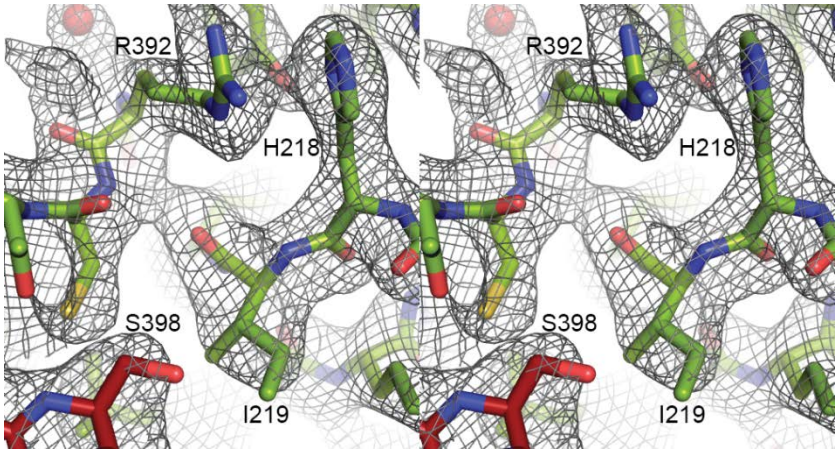
R392
H218
S398
I219
R392
H218
S398
I219

h

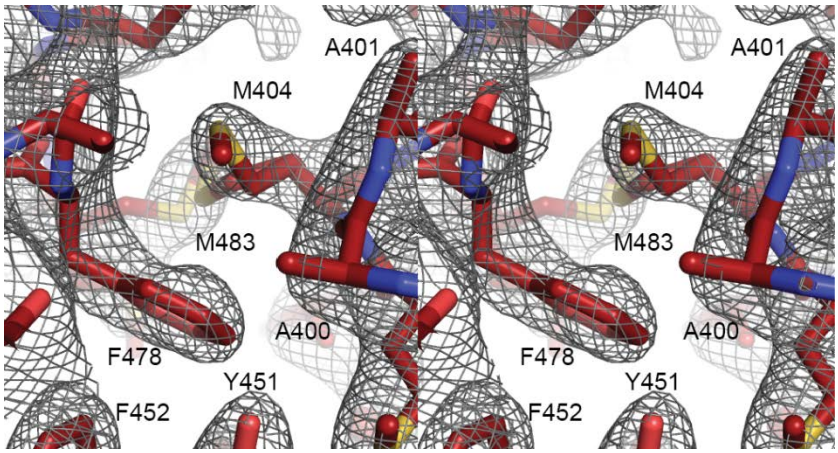
A401
M404
M483
A400
F478
Y451
F452
A401
M404
M483
A400
F478
Y451
F452

i

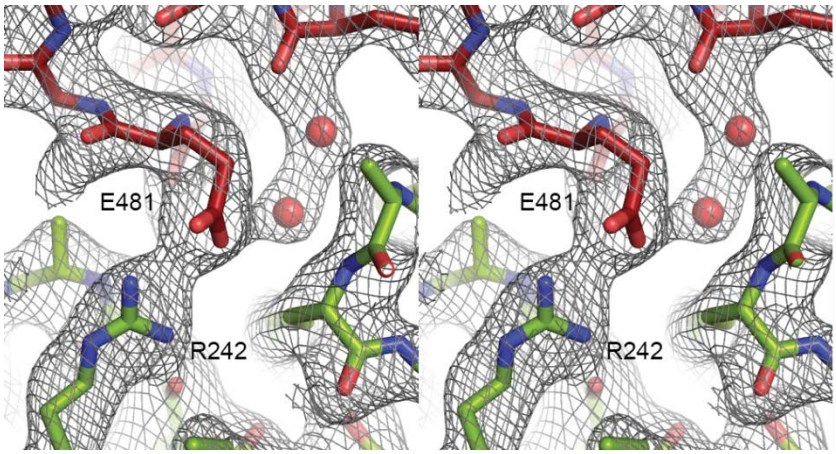
E481
R242
E481
R242

Supplementary Figure S5: Electron density maps for disease mutants

Stereo views of weighted 2FoFc electron density maps, contoured at 1σ cut-off, for the various mutant structures around the mutation sites and for RyR1BC at an arbitrary site, in the order as they appear in the manuscript. **a)** G249R (PDB ID: 4I1E) **b)** L14R (PDB ID: 4I7I) **c)** R45C (PDB ID: 4I6I) **d)** D61N (PDB ID: 4I3N) **e)** R402G (PDB ID: 4I37) **f)** C36R (PDB ID: 4I0Y) **g)** V219I (PDB ID: 4I8M) **h)** I404M (PDB ID: 4I2S) **i)** RyR1BC (PDB ID: 4I96)

Supplementary Figure S6: Domain reorientations are not due to pH differences

RyR1ABC wild-type structures crystallized at pH8.0 (white), pH9.0 (cream), and pH9.5 (orange) are superposed, based on domain A. The positions of domains B and C relative to domain A are unchanged, indicating that the changes observed for the disease mutants are not due to pH differences in the crystallization conditions.

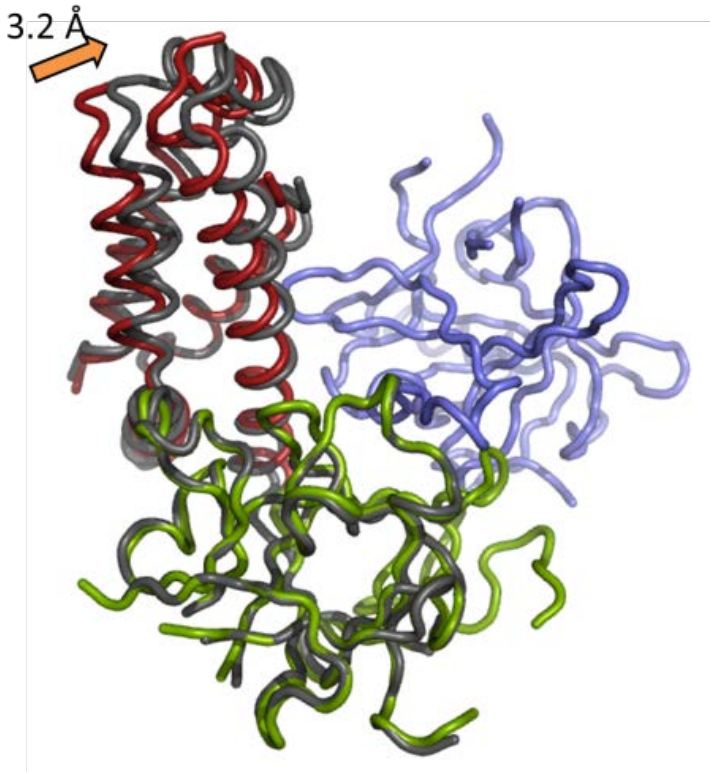

Supplementary Figure S7: The clamping action of domain A

Superposition of domains B of the RyR1BC and RyR1ABC crystal structures, showing the relative conformational changes of domain C (arrow). Gray: RyR1BC (PDB ID: 4I96). Colors: RyR1ABC domains A (blue), B (green), and C (red).

a **b**

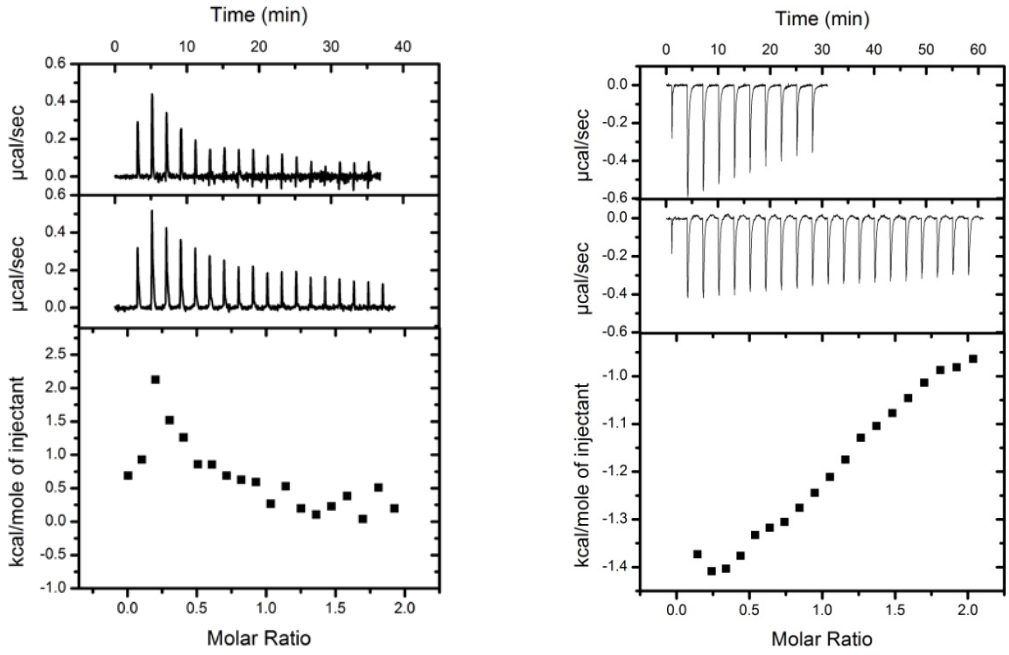

Supplementary Figure S8: Isothermal Titration Calorimetry

a) Titration of 1.63 mM FKBP12 into 163µM RyR1ABC. **b)** Titration of 2.65mM RyR1A into 265µM RyR1BC. In both cases, the top graph shows the background titration of the titrant into buffer, the middle graph shows the titrant into RyR1ABC or RyR1BC, and the bottom graph shows the integrated energies per mole of titrant for the middle graph. In both cases, the titrations are not significantly different from the background titrations, indicating that any trend line is due to dilution of the titrant. For the RyR1A – RyR1BC titration, the titrations would report on both the intrasubunit interactions (interfaces observed in the crystal structure), and on the proposed intersubunit interaction involving domains A and B. However, neither of the two interactions can be detected in solution, showing that both only arise in the context of full-length channels, where the effective concentration can be in the molar range.

Supplementary Table S1: Summary of functional characterizations of the mutants studied.

Mutation	Disease phenotype(s)	Primary identification references	Functional characterizations	Functional studies references
L14R	MH	[61]	Abnormally enhanced Ca^{2+}-induced Ca^{2+} release.	[61]
C36R	MH	[62]	Increased sensitivity to muscle contracture by caffeine. Increased sensitivities activation by caffeine and halothane.	[62] [63] [64]
R45C	MH	[65]	Increased sensitivity to muscle contracture by caffeine.	[65]
D61N	MH/CCD	[66] [67]	Assumed increased sensitivity of contraction to halothane, due to MH phenotype	
G216E	MH/CCD/MmD	[68] [69]	Assumed increased sensitivity of contraction to halothane, due to MH phenotype	
V219I	MH	[61]	Clearly enhanced Ca^{2+}-induced Ca^{2+} release.	[61]
G249R	MH	[70]	Increased sensitivities activation by caffeine and halothane. Increased sensitivities to activation by 4-CmC and Ca^{2+}. Decreased sensitivity to inactivation by Mg^{2+}.	[63] [64] [71]
R402G	MH	[66]	Assumed increased sensitivity of contraction to halothane, due to MH phenotype	
I404M	MH/CCD	[72]	Increased sensitivities activation by caffeine and halothane. Increased sensitivity to activation by depolarization.	[63] [64] [73]

Summary of functional characterizations of the mutants studied in this report, along with references for identification and characterization. All the mutants are associated with malignant hyperthermia (MH), which is known to cause gain-of-function phenotype in RyR1. Residue numbering is for rabbit RyR1. CCD = central core disease. MmD = multi-minicore disease.

Supplementary References

61. Ibarra, M.C. et al. Malignant hyperthermia in Japan: mutation screening of the entire ryanodine receptor type 1 gene coding region by direct sequencing. *Anesthesiology* **104**, 1146-1154 (2006).
62. Lynch, P.J. et al. Identification of heterozygous and homozygous individuals with the novel RYR1 mutation Cys35Arg in a large kindred. *Anesthesiology* **86**, 620-626 (1997).
63. Tong, J. et al. Caffeine and halothane sensitivity of intracellular Ca2+ release is altered by 15 calcium release channel (ryanodine receptor) mutations associated with malignant hyperthermia and/or central core disease. *J Biol Chem* **272**, 26332-26339 (1997).
64. Tong, J., McCarthy, T.V. & MacLennan, D.H. Measurement of resting cytosolic Ca2+ concentrations and Ca2+ store size in HEK-293 cells transfected with malignant hyperthermia or central core disease mutant Ca2+ release channels. *J Biol Chem* **274**, 693-702 (1999).
65. Tammaro, A. et al. Scanning for mutations of the ryanodine receptor (RYR1) gene by denaturing HPLC: detection of three novel malignant hyperthermia alleles. *Clin Chem* **49**, 761-768 (2003).
66. Robinson, R., Carpenter, D., Shaw, M.A., Halsall, J. & Hopkins, P. Mutations in RYR1 in malignant hyperthermia and central core disease. *Hum Mutat* **27**, 977-989 (2006).
67. Wu, S. et al. Central core disease is due to RYR1 mutations in more than 90% of patients. *Brain* **129**, 1470-1480 (2006).
68. Romero, N.B. et al. Dominant and recessive central core disease associated with RYR1 mutations and fetal akinesia. *Brain* **126**, 2341-2349 (2003).
69. Zhou, H., Treves, S., Jungbluth, H., Sewry, C. & Muntoni, F. RYR1 gene genotype-phenotype and functional correlative studies in central core disease and multi-minicore disease. *Neuromuscul Disord* **15**, 676-743 (2005).
70. Gillard, E.F. et al. Polymorphisms and deduced amino acid substitutions in the coding sequence of the ryanodine receptor (RYR1) gene in individuals with malignant hyperthermia. *Genomics* **13**, 1247-1254 (1992).
71. Sato, K., Pollock, N. & Stowell, K.M. Functional studies of RYR1 mutations in the skeletal muscle ryanodine receptor using human RYR1 complementary DNA. *Anesthesiology* **112**, 1350-1354 (2010).
72. Quane, K.A. et al. Mutations in the ryanodine receptor gene in central core disease and malignant hyperthermia. *Nat Genet* **5**, 51-55 (1993).
73. Avila, G. & Dirksen, R.T. Functional effects of central core disease mutations in the cytoplasmic region of the skeletal muscle ryanodine receptor. *J Gen Physiol* **118**, 277-290 (2001).